# From Triazines to Heptazines: Novel Nonmetal Tricyanomelaminates as Precursors for Graphitic Carbon Nitride Materials

Bettina V. Lotsch and Wolfgang Schnick*

*Department Chemie und Biochemie, Lehrstuhl für Anorganische Festkörperchemie, Ludwig-Maximilians-Universität München, Butenandtstrasse 5-13, D-81377 München, Germany*

*Received October 25, 2005. Revised Manuscript Received December 22, 2005*

The first non-metal tricyanomelaminates have been synthesized via metathesis reactions and characterized by means of single-crystal X-ray diffraction and vibrational and solid-state NMR spectroscopy. The crystal structures of $[NH_4]_2[C_6N_9H]$ (**1**) ($P2_1/c$, $a = 1060.8(2)$ pm, $b = 1146.2(2)$ pm, $c = 913.32(18)$ pm, $\beta = 112.36(3)°$, $V = 1027.0(4) \times 10^6$ pm$^3$), $[C(NH_2)_3]_3[C_6N_9]\cdot 2\ H_2O$ (**2**) ($P2_12_12_1$, $a = 762.12(15)$ pm, $b = 1333.6(3)$ pm, $c = 1856.6(4)$ pm, $V = 1887.0(7) \times 10^6$ pm$^3$) and $[C_3N_6H_7]_2[C_6N_9H]\cdot 2.5\ H_2O$ (**3**) ($P\bar{1}$, $a = 1029.5(2)$ pm, $b = 1120.3(2)$ pm, $c = 1120.7(2)$ pm, $\alpha = 104.22(3)°$, $\beta = 112.74(3)°$, $\gamma = 104.62(3)°$, $V = 1064.8(4) \times 10^6$ pm$^3$) are composed of singly protonated (**1** and **3**) or nonprotonated (**2**) tricyanomelaminate ions, which, together with the respective counterions, form two-dimensional, layered structures (**1** and **3**) or a quasi three-dimensional network (**2**). Particular emphasis has been placed on the elucidation of the thermal reactivity of the three molecular salts by means of thermal analysis and vibrational and NMR spectroscopy, as well as temperature-dependent X-ray powder diffraction. The title compounds were found to be promising candidates as molecular $CN_x$ precursors for the synthesis of graphitic carbon nitride materials. Upon being heated, ammonium and guanidinium tricyanomelaminate uniformly pass the crystalline, heptazine ($C_6N_7$)-based intermediate melem ($C_6N_7(NH_2)_3$), which decomposes and forms a semi-amorphous $CN_xH_y$ material with a pronounced layered structure. Identical pyrolysis products are obtained for the melaminium salt, a classical triazine ($C_3N_3$)-based $CN_x$ precursor, after passing an intermediate, possibly cross-linked phase at low temperatures. Preliminary solid-state NMR investigations of the final products best conform to heptazine-based structure models for g-$C_3N_4$ that have commonly been rather disregarded in favor of triazine-based ones.

## Introduction

In recent years, the significance of carbon nitride chemistry has predominantly been associated with the outstanding material properties predicted for 3D modifications of the binary representative $C_3N_4$.[1−13] Because of the inherent difficulties encountered in the synthesis of single-phase $sp^3$-hybridized modifications of $C_3N_4$ on a preparative scale by physical methods, the focus has shifted toward chemical approaches by taking advantage of the analogy to the graphite/diamond system: to date, innumerable experiments have been devised that utilize the condensation of suitable $CN_x$ precursors to form graphitic carbon nitride materials of general formula $CN_xH_y$.[1−3] The high-pressure conversion of these extended g-$C_3N_4$ structures is considered to be a viable approach to ultrahard 3 D carbon nitride, though it necessitates very high pressures still beyond those accessible by standard high-pressure techniques.[14−16] Apart from its significance as a prestage of diamondlike $C_3N_4$, graphitic carbon nitride is of current interest because of its promising mechanical, tribological, and optical properties.[17−20] Despite its emerging relevance in material science, progress in the chemistry of g-$C_3N_4$ is mainly driven by the empirical implementation of tailored material properties that are governed by particle size effects, texture, or nitrogen content.[21] As a result of its typical nonstoichiometry, varying hydrogen content, and largely amorphous character, the structure and bonding situation in graphitic carbon nitride has not been satisfactorily resolved yet. The most frequently

* To whom correspondence should be addressed. E-mail: wolfgang.schnick@uni-muenchen.de.

(1) Kroke, E.; Schwarz, M. *Coord. Chem. Rev.* **2004**, *248*, 493.
(2) Matsumoto, S.; Xie, E. Q.; Izumi, F. *Diamond Relat. Mater.* **1999**, *8*, 1175.
(3) Muhl, S.; Mendez, J. M. *Diamond Relat. Mater.* **1999**, *8*, 1809.
(4) Guo, Y.; Goddard, W. A., III. *Chem. Phys. Lett.* **1995**, *237*, 72.
(5) Sung, C.-M.; Sung, M. *Mater. Chem. Phys.* **1996**, *43*, 1.
(6) Cohen, M. L. *Phys. Rev. B* **1985**, *32*, 7988.
(7) Cohen, M. L. *Science* **1993**, *261*, 307.
(8) Liu, A. Y.; Cohen, M. L. *Science* **1989**, *245*, 841.
(9) Liu, A. Y.; Cohen, M. L. *Phys. Rev. B* **1990**, *41*, 10727.
(10) Niu, C.; Lu, Y. Z.; Lieber, C. M. *Science* **1993**, *261*, 334.
(11) Teter, D. M.; Hemley, R. J. *Science* **1996**, *271*, 53.
(12) Liu, A. Y.; Wentzcovich, R. M. *Phys. Rev. B.* **1994**, *50*, 10362.
(13) Ortega, J.; Sankey, O. F. *Phys. Rev. B.* **1995**, *51*, 2624.
(14) Teter, D. M.; Hemley, R. J. *Science* **1996**, *271*, 53.
(15) Kroll, P.; Hoffmann, R. *J. Am. Chem. Soc.* **1999**, *121*, 4696.
(16) Badding, J. V.; Nesting, D. C. *Chem. Mater.* **1996**, *8*, 535.
(17) Zhou, Z. B.; Cui, R. Q.; Pang, Q. J.; Hadi, G. M.; Ding, Z. M.; Li, W. Y. *Sol. Energy Mater. Sol. Cells* **2002**, *70*, 487.
(18) Sugimura, H.; Sato, Y.; Tajima, N.; Takai, O. *Surf. Coat. Technol.* **2001**, *142*, 714.
(19) Kulisch, W.; Popov, C.; Zambov, L. *New Diamond Front. Carbon Technol.* **2001**, *11*, 53.
(20) Grueger, H.; Kunath, C. PTC Int. Appl. WO 0369327 A1, Aug 21, 2003.
(21) Huynh, M. H. V.; Hiskey, M. A.; Archuleta, J. G.; Roemer, E. L. *Angew. Chem., Int. Ed.* **2005**, *44*, 737.

10.1021/cm052342f CCC: $33.50 
Published on Web 03/07/2006

**Scheme 1. Schematic Drawing of the Most Frequently Encountered Structure Propositions for g-$C_3N_4$**

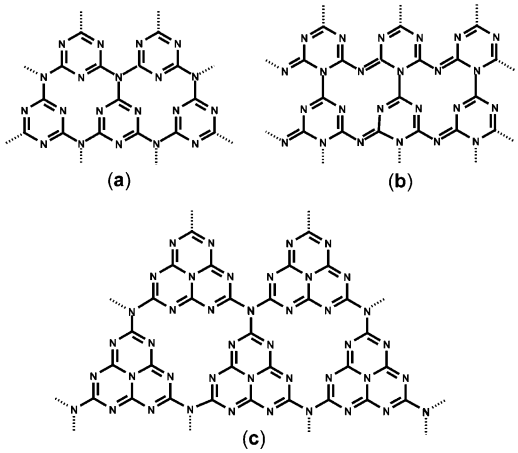


a) triazine-based, hexagonal; b) triazine-based, orthorhombic; c) heptazine-based network. The planarity of the layered condensation products is still a point of contention.

invoked structural model is based on the graphitic archetype; it is created formally by introducing ordered carbon vacancies into planar $(CN)_x$ sheets (Scheme 1a,b).[11,22−24] However, heptazine-based sheets that are structurally related to the hypothetical polymer melon[25−31] have recently been shown to be energetically favored with respect to the triazine-based modification (Scheme 1c).[32] Currently, both the actual existence of a graphitic material with idealized composition $C_3N_4$ and the true nature of its characteristic building blocks are still a matter of dispute. In particular, the hydrogen content reported in most studies is similar to that expected for melon (1.5 wt %), which casts some doubt on the current description of g-$C_3N_4$ as an extended 2D polymer with ideal 3:4 C:N stoichiometry. In the majority of cases, the structural building motives (triazine or heptazine) of the as-obtained $CN_xH_y$ materials are, therefore, simply interpreted in line with the nature of the respective starting materials.[33−38] To resolve this issue, we have to focus on the condensation pathways of suitable $CN_x$ precursors, thus deducing the structural building blocks of g-$C_3N_4$ from any possibly encountered intermediates.

Apart from melamine and melem,[36,39] a large variety of preferably nitrogen-rich triazine- or heptazine-based compounds that, at the same time, contain a minimum amount of hydrogen, such as triazido−triazine and −heptazine, cyanuric and cyameluric chloride, and N-functionalized 1,3,5-triazines,[23,38,40] as well as diamino-chloro-*s*-triazine[34,35,39,41−48] or molecular salts such as dicyanamides,[49−53] have been utilized as molecular $CN_x$ precursors. In addition, alternative high-temperature/high-pressure approaches have been devised that are predominantly based on solvothermal reactions with the solvents used under supercritical conditions.[24,43,54−56] Considering the above requirements, salts containing the tricyanomelaminate (TCM) anion represent particularly intriguing systems, because their cyanamide moieties are potentially susceptible to a versatile thermal solid-state reactivity. In previous works, the alkali salts of tricyanomelamine $M_3[C_6N_9]$ with M = Na−Rb have been prepared by utilizing the trimerization reaction of the respective dicyanamide salts $M[N(CN)_2]$ (M = Na−Rb).[57,58] In addition, the hydrated forms $M_3[C_6N_9]\cdot H_2O$ (M = Na, K, Rb) as well as hydrogentricyanomelaminates $M[HC_6N_9]\cdot 3H_2O$ (M = Co, Ni, Cu, Cd), $\{Co[H_2C_6N_9]_2(H_2O)_4\}\cdot 6H_2O$, and $Rb[H_2C_6N_9]\cdot 0.5H_2O$ were obtained by recrystallization of the parent tricyanomelaminates from acidic aqueous solutions.[59−63] Though they are stable up to temperatures around 773 K (K, Rb) or 873 K (Na), no information on the identity or the metal content of the amorphous thermolysis products is available. Attempts to synthesize the free acid tricyanomelamine in crystalline form invariably failed because of its inherent tendency toward polymerization.[64,65] With the introduction

(22) Mattesini, M.; Matar, S. F.; Etourneau, J. *J. Mater. Chem.* **2000**, *10*, 709.
(23) Wang, J.; Miller, D. R.; Gillan, E. G. *Carbon* **2003**, *41*, 2031.
(24) Alves, I.; Demazeau, G.; Tanguy, B.; Weill, F. *Solid State Commun.* **1999**, *109*, 697.
(25) Liebig, J. v. *Ann. Pharm.* **1834**, *10*, 10.
(26) Gmelin, L. *Ann. Pharm.* **1835**, *15*, 252.
(27) Liebig, J. v. *Ann. Chem. Pharm.* **1850**, *50*, 337.
(28) Liebig, J. v. *Ann. Chem. Pharm.* **1850**, *73*, 257.
(29) Franklin, E. C. *J. Am. Chem. Soc.* **1922**, *44*, 486.
(30) May, H. J. *Appl. Chem.* **1959**, 340.
(31) Komatsu, T. *Macromol. Chem. Phys.* **2001**, *202*, 19.
(32) Kroke, E.; Schwarz, M.; Horath-Bordon, E.; Kroll, P.; Noll, B.; Norman, A. D. *New J. Chem.* **2002**, *26*, 508.
(33) Miller, D. R.; Wang, J.; Gillan, E. G. *J. Mater. Chem.* **2002**, *12*, 2463.
(34) Guo, Q.; Xie, Y.; Wang, X.; Zhang, S.; Hou, T.; Lv, S. *Chem. Commun.* **2004**, 26.
(35) Guo, Q.; Xie, Y.; Wang, X.; Lv, S.; Hou, T.; Liu, X. *Chem. Phys. Lett.* **2003**, *380*, 84.
(36) Komatsu, T. *J. Mater. Chem.* **2001**, *11*, 799.
(37) Komatsu, T.; Nakamura, T. *J. Mater. Chem.* **2001**, *11*, 474.
(38) Kouvetakis, J.; Bandari, A.; Todd, M.; Wilkens, B. *Chem. Mater.* 1994, *6*, 811.
(39) Jürgens, B.; Irran, E.; Senker, J.; Kroll, P.; Müller, H.; Schnick, W. *J. Am. Chem. Soc.* **2003**, *125*, 10288.
(40) Todd, M.; Kouvetakis, J.; Groy, T. L.; Chandrasekhar, D.; Smith, D. J.; Deal, P. W. *Chem. Mater.* **1995**, *7*, 1422.
(41) Gillan, E. G. *Chem. Mater.* **2000**, *12*, 3906.
(42) Miller, D. R.; Swenson, D. C.; Gillan, E. G. *J. Am. Chem. Soc.* **2004**, *126*, 5372.
(43) Courjault, S.; Tanguy, B.; Demazeau, G. *C. R. Acad. Sci., Ser. IIc: Chim.* **1999**, *2*, 487.
(44) Khabashesku, V. N.; Zimmerman, J. L.; Margrave, J. L. *Chem. Mater.* **2000**, *12*, 3264.
(45) Vodak, D. T.; Kim, K.; Iordanidis, L.; Rasmussen, P. G.; Matzger, A. J.; Yaghi, O. M. *Chem.—Eur. J.* **2003**, *9*, 4197.
(46) Zhang, Z. H.; Leinenweber, K.; Bauer, M.; Garvie, L. A. J.; McMillan, P. F.; Wolf, G. H. *J. Am. Chem. Soc.* **2001**, *123*, 7788.
(47) Kawaguchi, M.; Nozaki, K. *Chem. Mater.* **1995**, *7*, 257.
(48) Zimmermann, J. L.; Williams, R.; Khabashesku, N.; Margrave, J. L. *Nano Lett.* **2001**, *1*, 731.
(49) Jürgens, B.; Höppe, H. A.; Irran, E.; Schnick, W. *Inorg. Chem.* **2002**, *41*, 4849.
(50) Lotsch, B. V.; Senker, J.; Kockelmann, W.; Schnick, W. *J. Solid State Chem.* **2003**, *176*, 180.
(51) Lotsch, B. V.; Senker, J.; Schnick, W. *Inorg. Chem.* **2004**, *43*, 895.
(52) Lotsch, B. V.; Schnick, W. *New J. Chem.* **2004**, *28*, 1129.
(53) Lotsch, B. V.; Schnick, W. *Chem. Mater.* **2005**, *17*, 3976.
(54) Montigaud, H.; Tanguy, B.; Demazeau, G.; Alves, I.; Courjault, S. *J. Mater. Sci.* **2000**, *35*, 2547.
(55) Montigaud, H.; Tanguy, B.; Demazeau, G.; Alves, I.; Birot, M.; Dunogues, J. *Diamond Relat. Mater.* **1999**, *8*, 1707.
(56) Demazeau, G. *J. Mater. Chem.* **1999**, *9*, 15.
(57) Jürgens, B.; Irran, E.; Schneider, J.; Schnick, W. *Inorg. Chem.* **2000**, *39*, 665.
(58) Irran, E.; Jürgens, B.; Schnick, W. *Chem.—Eur. J.* **2001**, *7*, 5372.
(59) Jürgens, B.; Milius, W.; Morys, P.; Schnick, W. *Z. Anorg. Allg. Chem.* **1998**, *624*, 91.
(60) Irran, E.; Jürgens, B.; Schnick, W. *Solid State Sci.* **2002**, *4*, 1305.
(61) Abrahams, B. F.; Egan, S. J.; Hoskins, B. F.; Robson, R. *Chem. Commun.* **1996**, 1099.
(62) Abrahams, B. F.; Egan, S. J.; Hoskins, B. F.; Robson, R. *Acta Crystallogr., Sect. C* **1996**, *52*, 2427.
(63) Jürgens, B.; Höppe, H. A.; Schnick, W. *Z. Anorg. Allg. Chem.* **2004**, *630*, 35.

of nonmetal $CN_xH_y$-based counterions, tricyanomelaminates may represent triazine-based, thermally reactive model systems that possess potential relevance as carbon nitride precursors. In particular, the presence of moderately acidic complex cations provides a means of in situ formation of the free acid tricyanomelamine, which may further undergo condensation processes toward triazine-based extended polymers, possibly involving the reactive cyanamide moieties.

In the following, we present the synthesis and structural characterization of the first nonmetal tricyanomelaminates. Although we conceptually place the systems under study in the context of $CN_x$ precursor chemistry, the focus will be on the relevance of their thermal reactivity with respect to the structural identity of g-$C_3N_4$.

## Experimental Section

**Synthesis.** Sodium−TCM was prepared according to a method described elsewhere.[57,59]

Ammonium−TCM (**1**) and guanidinium−TCM (**2**) were synthesized by ion-exchange reactions. In a typical procedure, an aqueous solution of the respective chloride (XCl, X = $NH_4$, $C(NH_2)_3$; Fluka, ≥98%, 3.0−3.5 M) was poured on a column containing an ion-exchange resin in strongly acidic form (20 mL, Ionenaustauscher I, $H^+$-Form, Art. 4765, Merck). After the column was fully loaded, the exchange resin was washed thoroughly with deionized water and the removal of excess chloride was substantiated by the $AgNO_3$ method. Subsequently, a solution of sodium−TCM (610 mg/30 mL $H_2O$ (**1**) or 940 mg/30 mL $H_2O$ (**2**)) was poured on the column and the eluate was evaporated at room temperature. The product of the ammonium−TCM synthesis was found to be strongly dependent on the concentration of the sodium−TCM solution. Reducing the concentration from 0.10 to 0.06 M resulted in the formation of a metastable hydrated phase, which gradually dehydrated when exposed to air at ambient temperature. Details concerning the stability and structure of the hydrated ammonium−TCM will be treated separately in a forthcoming paper. Guanidinium−TCM was always obtained as a two-phase mixture composed of colorless crystals of **2** and ball-shaped aggregates of a white polycrystalline powder. Judging from its vibrational and solid-state NMR spectra, we may describe the latter phase as $[C(NH_2)_3]_2[C_6N_6H]\cdot xH_2O$. However, no single-crystals have been isolated yet.

Melaminium−TCM (**3**) was prepared by adding a solution of sodium−TCM (207 mg, 0.78 mmol) to a hot 1:3 methanol:water solution (400 mL) of melaminium sulfate $[C_3N_6H_7]_2[SO_4]\cdot 2H_2O$ (500 mg, 1.30 mmol). The solution was kept at 353 K until crystallization commenced.

Melaminium sulfate was prepared by adding 16% $H_2SO_4$ (30 mL) to 270 mL of a hot aqueous solution of melamine (≥99%, Fluka, 3.0 g, 23.80 mmol). The solution was cooled slowly, and the obtained crystals were filtered off.

$^{15}$N melamine was prepared according to a procedure described in detail elsewhere.[39]

Data for **1**: IR (KBr) $\nu$ = 3456.8, 3237.0, 3051.4, 2840.9 $cm^{-1}$ (s, $\nu$O−H, $\nu$N−H), 2182.7 $cm^{-1}$ (vs, $\nu$N−C≡N), 1576.3 $cm^{-1}$ (vs, $\delta$N−H), 1532.4 $cm^{-1}$ (vs, $\nu CN_{ring}$), 1456.3, 1438.5, 1408.2, 1392.6, 1334.5 $cm^{-1}$ (vs, $\delta CN_{ring}$ + $\nu$C−NCN), 1215.5 $cm^{-1}$ (w, $\nu$NCN + ($\delta CN_{ring}$)), 1027.5 $cm^{-1}$ (w, $\delta$skeleton + ($\delta$NCN)), 980.4 $cm^{-1}$ (w, $\delta C_3N_3$), 788.9 $cm^{-1}$ (w, $\gamma_s C_3N_3$), 760.6 $cm^{-1}$ (w, $\omega$N−H), 747.9 $cm^{-1}$ (w, $\gamma_{as} C_3N_3$), 698.9 $cm^{-1}$ (w, $\delta$NCN + $\delta C_3N_3$), 570.1, 549.9 $cm^{-1}$ (w, $\gamma$NCN). Anal. Calcd (in wt %) for $[(NH_4)_2][C_6N_9H]$ (**1**): C, 30.63; N, 65.51; H, 3.86. Found: C, 30.57; N, 65.68; H, 4.01.

Data for **2**: IR (KBr) $\nu$ = 3333.1, 3133.0 $cm^{-1}$ (s, $\nu$O−H, $\nu$N−H), 2132.8 $cm^{-1}$ (vs, $\nu$N−C≡N), 1669.6 $cm^{-1}$ (vs, $\nu$C=N, $\delta$N−H, $\delta$O−H), 1580.4 $cm^{-1}$ (w, $\delta$N−H), 1474.5 $cm^{-1}$ (vs, $\nu CN_{ring}$), 1389.6 $cm^{-1}$ (vs, $\delta CN_{ring}$ + $\nu$C−NCN), 1249.8, 1145.5 $cm^{-1}$ (w, $\nu$NCN + ($\delta CN_{ring}$)), 1006.5 $cm^{-1}$ (vw, $\delta$skeleton + ($\delta$NCN)), 985.6 $cm^{-1}$ (vw, $\delta C_3N_3$), 814.5 $cm^{-1}$ (m, $\gamma C_3N_3$), 582.5 $cm^{-1}$ (w, $\gamma$NCN). Anal. Calcd (in wt %) for $[C(NH_2)_3]_3[C_6N_9]\cdot 2H_2O$ (**2**): C, 26.08; N, 60.84; H, 5.36. Found: C, 26.11; N, 61.05; H, 5.26.

Data for **3**: IR (KBr) $\nu$ = 3358.5, 3138.5, 2908.0, 2728.3 $cm^{-1}$ (s, $\nu$O−H, $\nu$N−H), 2182.7 $cm^{-1}$ (vs, $\nu$N−C≡N), 1667.6 $cm^{-1}$ (vs, $\nu CN_{ring,}$ melamine, $\delta$N−H, $\delta$O−H), 1580.7 $cm^{-1}$ (vs, $\delta$N−H), 1506.7 $cm^{-1}$ (vs, $\nu CN_{ring,}$ TCM), 1413.7, 1377.5 $cm^{-1}$ (vs, $\delta CN_{ring,}$ TCM + $\nu$C−NCN), 1178.2 $cm^{-1}$ (w, $\nu$NCN + ($\delta CN_{ring,\ TCM}$)), 1031.7 $cm^{-1}$ (w, $\delta$skeleton + ($\delta$NCN)), 975.5 $cm^{-1}$ (w, $\delta C_3N_3$), 782.4 $cm^{-1}$ (m, $\gamma_s C_3N_3$), 746.1 $cm^{-1}$ (vw, $\gamma_{as} C_3N_3$), 697.7 $cm^{-1}$ (vw, $\delta$NCN + $\delta C_3N_3$), 568.0 $cm^{-1}$ (w, $\gamma$NCN, ring $bend_{melamine}$). Anal. Calcd (in wt %) for $[(C_3N_6H_7)_2][C_6N_9H]\cdot 2.4H_2O$ (**3**): C, 28.91; N, 59.02; H, 4.05. Found: C, 28.78; N, 58.99; H, 4.12. MS (ESI$^-$) *m/z* (%) = 200.05 (100) $[A + H]^-$, 222.04 (20) $[A + Na]^-$, 423.09 (45) $[2A + 2H + Na]^-$; (DEI$^+$) *m/z* (%) = 126.10 (12) $[C_3N_6H_6]^+$.

**General Methods.** Direct insertion DEI$^+$ (70 eV) mass spectra were obtained using a JEOL MStation JMS-700 gas inlet system. Electrospray ionization (ESI) measurements were conducted on a Finnigan MAT 95Q and a Finnigan MAT 90 mass spectrometer using an API−Interface II with ESI probe head and a capillary voltage of 2.5 kV.

Elemental analyses were performed using a commercial Vario EL C, H, N elemental analyzer system (Elementar Analysensysteme GmbH).

**X-ray-Diffraction.** X-ray diffraction data of **1** were recorded on a STOE IPDS diffractometer; single crystals of **2** and **3** were measured on an ENRAF-NONIUS Kappa CCD diffractometer equipped with a rotating anode using graphite-monochromated Mo Kα radiation ($\lambda$ = 71.073 pm). The crystal structures were solved by direct methods using the program SHELXS-97[66] and refined on $F^2$ by applying the full-matrix least-squares method implemented in SHELXL-97.[67] No absorption corrections were carried out because of the weak absorption coefficients of the constituent atoms. The positions of all hydrogen atoms were determined from difference Fourier syntheses. The hydrogen positions in **3** were subsequently refined using a riding model (NH, $NH_2$) or with the distances and angles restrained to be equal (crystal water). All non-hydrogen atoms were refined anisotropically. Details of the crystal structure determinations and refinements are summarized in Table 1. Crystallographic data for the structures have been deposited with the Cambridge Crystallographic Data Centre as CCDC-287126 (**1**), CCDC-287124 (**2**), and CCDC-287125 (**3**). Copies of the data can be obtained free of charge on application to the director, CCDC, 12 Union Road, Cambridge CB2 1EZ, UK. (Fax: int.code +(1223)-336-033. E-mail for inquiry: fileserv@ccdc.cam.ac.uk. E-mail for deposition: deposit@ccdc.cam.ac.uk.)

X-ray diffraction experiments on powder samples at room temperature were conducted on a STOE Stadi P diffractometer with Ge(111)-monochromated Cu Kα1 radiation ($\lambda$ = 154.06 pm).

High-temperature in situ X-ray diffractometry was performed on a STOE Stadi P powder diffractometer (Ge(111)-monochromated

(64) Jürgens, B. Ph.D. Thesis, University of Munich, Germany, 2004; Shaker Verlag: Aachen, Germany, 2004.
(65) Madelung, W.; Kern, E. *Liebigs Ann. Chem.* **1922**, *427*, 1.
(66) Sheldrick, G. M. *SHELXS97, Program for the Solution of Crystal Structures*; University of Göttingen: Göttingen, Germany, 1997.
(67) Sheldrick, G. M. *SHELXL97, Program for the Refinement of Crystal Structures*; University of Göttingen: Göttingen, Germany, 1997.

**Table 1. Selected Crystallographic Data and Structure Refinement of Tricyanomelaminate Salts 1, 2, and 3**

| | $[NH_4]_2[C_6N_9H]$ (**1**) | $[C(NH_2)_3]_3[C_6N_9]\cdot 2H_2O$ (**2**) | $[C_3N_6H_7]_2[C_6N_9H]\cdot 2.4H_2O$ (**3**) |
|---|---|---|---|
| molar mass (g mol$^{-1}$) | 235.24 | 414.45 | 496.69 |
| cryst syst | monoclinic | orthorhombic | triclinic |
| space group | $P2_1/c$ (No. 14) | $P2_12_12_1$ (No.19) | $P\bar{1}$ (No.2) |
| $T$ (K) | 200 | 200 | 200 |
| diffractometer, monochromator | STOE IPDS, graphite | Enraf-Nonius Kappa CCD, graphite | Enraf-Nonius Kappa CCD, graphite |
| radiation, $\lambda$ (pm) | Mo K$\alpha$, 71.073 | Mo K$\alpha$, 71.073 | Mo K$\alpha$, 71.073 |
| $Z$ | 4 | 4 | 2 |
| $a$ (pm) | 1060.8(2) | 762.12(15) | 1029.5(2) |
| $b$ (pm) | 1146.2(2) | 1333.6(3) | 1120.3(2) |
| $c$ (pm) | 913.32(18) | 1856.6(4) | 1120.7(2) |
| $\alpha$ (deg, $\neq 90°$) | | | 104.22(3) |
| $\beta$ (deg, $\neq 90°$) | 112.36(3) | | 112.74(3) |
| $\gamma$ (deg, $\neq 90°$) | | | 104.62(3) |
| $V$ ($\times 10^6$, pm$^3$) | 1027.0(4) | 1887.0(7) | 1064.8(4) |
| calcd density (g cm$^{-3}$) | 1.521 | 1.459 | 1.555 |
| cryst size (mm$^3$) | 0.29 × 0.19 × 0.17 | 0.49 × 0.35 × 0.30 | 0.30 × 0.14 × 0.04 |
| abs coeff (mm$^{-1}$) | 0.113 | 0.113 | 0.121 |
| diffraction range (deg) | $2.73 \le \theta \le 27.49$ | $3.25 \le \theta \le 27.44$ | $3.44 \le \theta \le 26.00$ |
| index range | $-13 \le h \le 13$, $-14 \le k \le 14$, $-11 \le l \le 11$ | $-9 \le h \le 9$, $-17 \le k \le 17$, $-24 \le l \le 24$ | $-12 \le h \le 12$, $-13 \le k \le 13$, $-13 \le l \le 13$ |
| params/restraints | 190/0 | 351/0 | 345/9 |
| total no. of reflns | 8307 | 24736 | 12076 |
| no. of independent reflns | 2257 | 4274 | 4111 |
| no. of observed reflns | 1640 ($R_{int} = 0.0475$) with ($F_o^2 \ge 2\sigma F_o^2$) | 4077 ($R_{int} = 0.0371$) with ($F_o^2 \ge 2\sigma F_o^2$) | 2671 ($R_{int} = 0.0443$) with ($F_o^2 \ge 2\sigma F_o^2$) |
| GOF on $F^2$ | 0.914 | 1.087 | 1.026 |
| final R1 indices [$I > 2\sigma(I)$] (all data) | 0.0295 (0.0471) | 0.0253 (0.0277) | 0.0570 (0.1015) |
| final wR2 indices [$I > 2\sigma(I)$] (all data) | 0.0680 (0.0721)[a] | 0.0652 (0.0666)[b] | 0.1230 (0.1458)[c] |
| min./max. residual electron density ($\times 10^{-6}$, e pm$^{-3}$) | −0.153/0.166 | −0.181/0.113 | −0.537/0.481 |

[a] $w = [\sigma^2(F_o^2) + (0.0435P)^2 + 0.0000P]^{-1}$, where $P = (F_o^2 + 2F_c^2)/3$. [b] $w = [\sigma^2(F_o^2) + (0.0372P)^2 + 0.1866P]^{-1}$, where $P = (F_o^2 + 2F_c^2)/3$. [c] $w = [\sigma^2(F_o^2) + (0.0496P)^2 + 0.9337P]^{-1}$, where $P = (F_o^2 + 2F_c^2)/3$.

Mo K$\alpha$1 radiation, $\lambda = 70.093$ pm) with an integrated furnace, using unsealed quartz capillaries (∅ 0.5 mm) as sample containers. The data collection was restricted to a $2\theta$ range of approximately 3−16° and an average scan-collection time of 34 min. The samples were heated from 323 K to temperatures around 923 K in steps of 10 K min$^{-1}$, using a heating rate of 20 K min$^{-1}$ between the scans.

**Solid-State NMR Spectroscopy.** $^{15}$N CP-MAS solid-state NMR spectra were recorded at ambient temperature on a DSX 500 Avance conventional impulse spectrometer (Bruker) operating at 500 MHz. The samples were contained in 4 mm $ZrO_2$ rotors, which were mounted in a standard double-resonance MAS probe head (Bruker). The $^{15}$N signals were referenced with respect to nitromethane.

A ramped cross-polarization sequence was employed to excite the $^{15}$N nuclei via a proton bath, where the power of the $^1$H radiation was linearly varied about 50%. A CPPI (cross-polarization combined with polarization inversion) experiment was performed to probe the number of hydrogen atoms directly attached to the nitrogen atoms[68] present in sample **3**, with an inversion time of 100 $\mu$s and a contact time of 2 ms. The recycle delay was fixed at 5 s, as derived from $^1$H T1 measurements. In the CP experiments, contact times of 20 ms (**1**) and 10 ms (**3**) were used and the recycle delays were 1 s (**1**) and 5 s (**3**). Sample spinning frequencies of 10 kHz and 5 kHz for CP and CPPI experiments, respectively, were employed. The data collection of all experiments was performed by applying broadband proton decoupling using a TPPM sequence.[69]

**Vibrational Spectroscopy.** FTIR measurements were carried out on a Bruker IFS 66v/S spectrometer. Spectra of the samples were recorded as KBr pellets (1 mg sample, 500 mg KBr) at ambient conditions between 400 and 4000 cm$^{-1}$.

**Thermal Analysis.** Thermoanalytical measurements between room temperature and 800 K were conducted on a Mettler DSC 25 with a heating rate of 1 K min$^{-1}$. The aluminum crucible used as the sample container was placed in the calorimeter under an atmosphere of dry nitrogen. The thermal behavior of the tricyanomelaminates was studied in a preparative scale by heating 40−80 mg of the substances in sealed glass or quartz ampules (10−12 cm) to various temperatures between 373 and 893 K, using a heating rate of 1 K min$^{-1}$ and analyzing the products by X-ray powder diffraction, IR, and solid-state NMR spectroscopy.

## Results and Discussion

**Crystal Structures and Spectroscopic Characterization.** Though closely related with respect to their saltlike structures and basic composition, some of the characteristic differences encountered in the crystal structures of **1**, **2**, and **3** are outlined in Figure 1. Although the tricyanomelaminate anion in the ammonium ($P2_1/c$) and melaminium salts ($P\bar{1}$) is singly protonated, the guanidinium salt ($P2_12_12_1$) contains a nonprotonated anionic core. Accordingly, in **1** and **3**, two ammonium or singly protonated melaminium ions, respectively, function as charge compensating cations, whereas three guanidinium residues are present in **2**. The anions in **1** and **3** possess $C_s$ geometry, whereas in **2**, the noncrystallographic point symmetry of the tricyanomelaminate anion is approximately represented by $C_{3h}$. This motif may be attributable to the steric requirements of the proton with respect to the adjacent cyanamide moieties. Although nonprotonated tricyanomelaminate salts with anions possessing $C_s$ symmetry are known,[57,58,64] the latter point symmetry could be enforced by the cyanamide moieties by avoiding the proton attached to the triazine core between them. The

(68) Gervais, C.; Babonneau, F.; Maquet, J.; Bonhomme, C.; Massiot, D.; Framery, E.; Vaultier, M. *Magn. Res. Chem.* **1998**, *36*, 407.

(69) Bennett, A. E.; Rienstra, C.; Auger, M.; Lakshmi, K. V.; Griffin, R. G. *J. Chem. Phys.* **1995**, *103*, 6951.

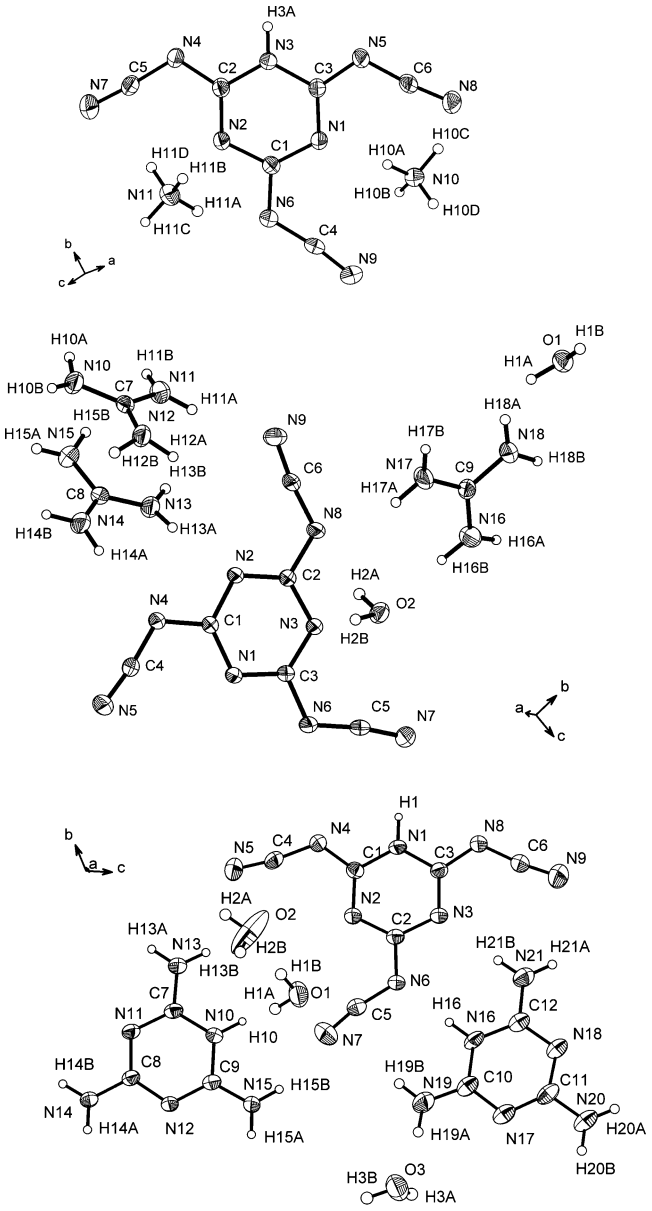


**Figure 1.** Representation of one formula unit of the unit cells of **1** (top), **2** (middle), and **3** (bottom). Thermal displacement ellipsoids (except for H) are drawn at the 50% probability level.

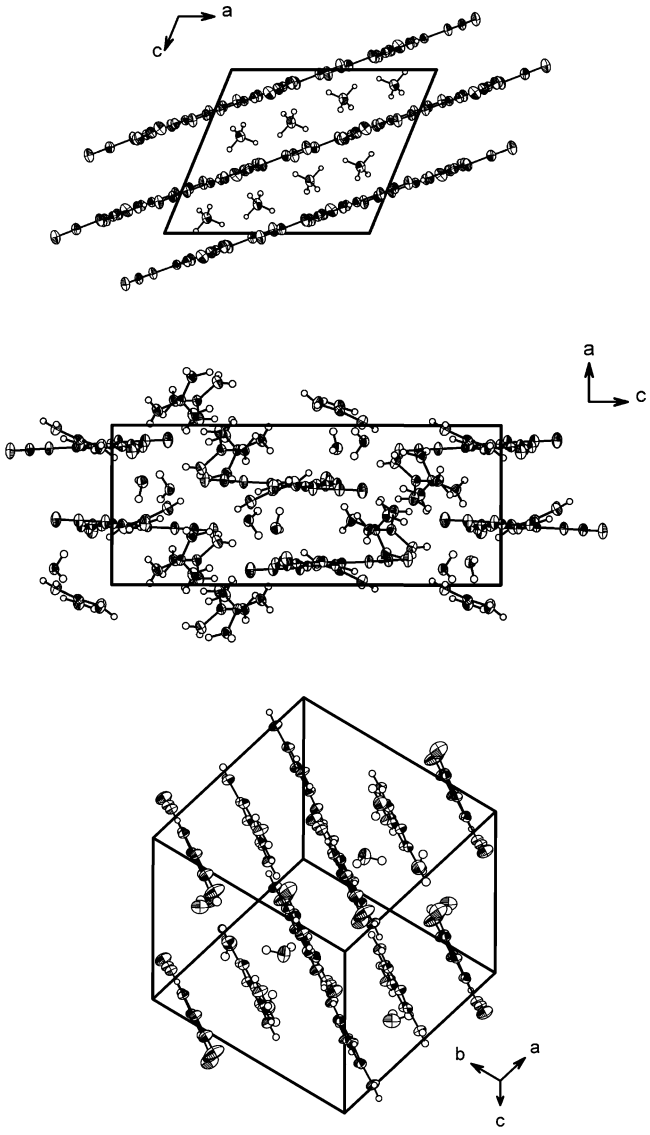


**Figure 2.** Unit cells of **1** (top), **2** (middle), and **3** (bottom) that clarify the pronounced layered structures of **1** and **3** in contrast to the spatially extended, nonlayered structure that results from mutual tilting of the guanidinium and TCM residues in **2**. Thermal displacement ellipsoids (except for H) are drawn at the 50% probability level.

guanidinium and melaminium salts both contain crystal water, which is largely disordered (O2) or has a site occupation factor ≤1 (O3) in the latter case (**3**). This effect may predominantly be rationalized by the pronounced layered structure of **3**, where the water molecules are loosely embedded between the layers, linking them by hydrogen bridges. A similar effect can be observed in **1** when formally exchanging the water molecules with ammonium ions (Figure 2). Therefore, whereas the sheets in **1** are solely composed of anions linked by weak hydrogen bonds (N8···H3A = 223 pm), with the cations functioning as connectors, the layers in **3** are made up by both cations and anions, which, because of their similar shape, smoothly pack into an extended two-dimensional array. The latter arrangement is fixed by medium-strong to weak intralayer hydrogen bonding contacts (N/O···H = 184−259 pm) with donor−acceptor distances ranging between 274 and 347 pm. The water molecules are either inserted between the layers (O1) or serve as cross linkers within the sheets (O2/O3). The interlayer distances in both **1** and **3** amount to approximately 350 pm (327 pm in melem),[39] which is on the same order of magnitude as the typical value expected for extended graphitic $CN_x$ structures (310−350 pm).[70] In contrast, **2** is composed of cations, anions, and crystal water mutually linked by hydrogen bridges (N/O···H = 194−262 pm) into a quasi-three-dimensional array (Figure 2).

The local structural parameters for both the cations and anions in **1**−**3** largely coincide with those from literature data.[57−64] According to expectations, the backbones of the monoprotonated tricyanomelaminate rings show greater variations in the C−N bond lengths (**1**, 133−137 pm; **3**, 133−136 pm) than does the nonprotonated anion in **2** (135 pm). The bond lengths of all cyanamide moieties are consistent with adjacent single (131−133 pm) and triple

(70) Mattesini, M.; Matar, S. F.; Snis, A.; Etourneau, J.; Mavromaras, A. *J. Mater. Chem.* **1999**, *9*, 3151.

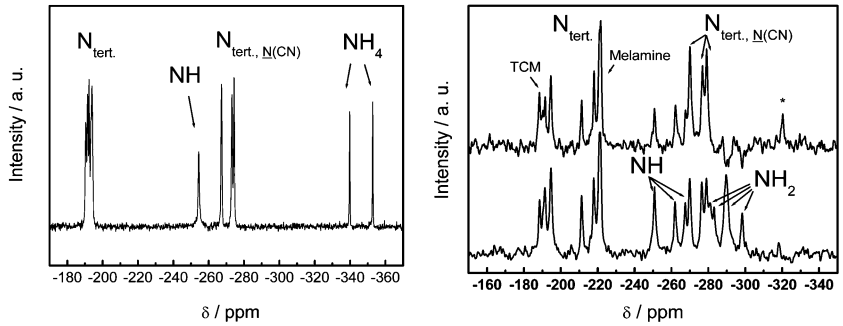


**Figure 3.** $^{15}$N MAS solid-state NMR spectra of **1** (left) and **3** (right). For **1**, all assignments were made on the basis of a CP experiment; in the case of **3**, a CPPI experiment was performed as well (top spectrum, right, see the text for further details). Spinning sidebands are marked by asterisks.

bonds (115−116 pm) exhibiting a significant degree of delocalization of the electron density along the slightly bent N−C≡N entities (∠170−176°). In addition to the X-ray structure analysis, the local structures of **1** (left) and **3** (right) were probed independently by $^{15}$N MAS solid-state NMR (Figure 3). The acquisition of high-resolution chemical shift spectra by applying fast MAS conditions allows may be complemented by spectral editing techniques such as the CPPI impulse sequence. This experiment permits the identification of $^{15}$N sites according to their proton environments. Thus, the unambiguous assignment of the $^{15}$N signals to primary, secondary, and tertiary nitrogen atoms is feasible.[39,68] As shown in Figure 3, all nitrogen resonances can be assigned on account of their isotropic chemical shift spectrum for **1** (left) and **3** (right, bottom), as well as by their polarization behavior in the case of **3**, as expressed by the relative intensities in the CPPI experiment (right, top). The theoretical normalized polarization inversion curves for the $NH_n$ groups are dominated by two time regimes, the crossover between which is observable at a normalized intensity given by $[2/(n + 1)] - 1$ ($n = 0-2$).[39,68] For the particular inversion time chosen in this experiment (100 $\mu$s), the normalized intensity of the NH groups (crossover at 0) is expected to be slightly positive, whereas that of $NH_2$ groups (crossover at −1/3) is expected to be negative; that of tertiary N atoms should be decreased only slightly, according to previous studies.[39,68] Thus, the CPPI experimental data allow for the accurate correlation of the observed resonances with the according $NH_n$ moieties: as demonstrated in Figure 3 (right, top), the experimental intensities of the tertiary nitrogen sites are in fact essentially unaffected, whereas the magnetization of the NH moieties has dropped significantly, although it is still positive. According to theory, the signals arising from the $NH_2$ groups are close to the zero-crossing, yet with inverted signs, all of which coincide with the crystallographic data.

The quantification of the intensities extracted from CP experiments, however, must be inherently inaccurate because of the different cross-polarization dynamics of chemically inequivalent $^{15}$N sites. Nevertheless, comparison of the experimental spectrum with the chemical shift and number of signals theoretically expected for the crystallographic asymmetric units provides independent support for the adequacy of the molecular structures and local symmetry as derived from X-ray analysis.

**Thermal Behavior.** In view of the identity of the model compounds established above, an interesting aspect of their thermal behavior relates to the possible conservation of the triazine ring systems upon heating. Because of the largely amorphous character of the as-formed polymeric $CN_xH_y$ materials and the spectroscopic similarities of triazine and heptazine systems, unequivocally resolving this issue by a combination of diffraction techniques and vibrational spectroscopy is still out of reach. However, by shifting the focus to the intermediates formed during the pyrolyses, it may nevertheless be possible for us to make basic conclusions concerning the structures of the polymeric materials.

In principle, similar condensation pathways of ammonium−, guanidinium−, and melaminium−TCM can be envisaged due to the (albeit gradually differing) acidity of the respective cations. As previously observed for related systems,[50−53] a proton transfer from the cation to the tricyanomelaminate anion may initiate thermal condensation, thereby releasing the thus-formed neutral species either as gas ($NH_3$) or as potentially nucleophilic agents ($(H_2N)_2C{=}NH$ and $C_3N_6H_6$) in further thermally induced reaction steps. The in situ generated free acid tricyanomelamine, which is liable to oligomerization or polymerization,[64,65] may then form highly condensed triazine-based species, as sketched for the ammonium salt (**1**) (Scheme 2) as an example. Analogously, the release of free melamine that possesses nucleophilic sites in **3** in the presence of electrophilic cyanamide groups of TCM may contribute to the formation of triazine-based networks.

**DSC and In Situ X-ray Diffraction.** The principal succession of thermal events in the pyrolysis processes of the title compounds was followed by DSC measurements (Figure 4). Both **2** and **3** exhibit pronounced endothermic signals between 380 and 425 K, which may be attributed to the loss of crystal water. The splitting of the signals may be due to the stepwise release of ∼2.4 (**3**) or 2 (**2**) molecules of $H_2O$ per formula unit. Accordingly, temperature-programmed X-ray diffractometry (TPXRD) clearly shows that the respective conversions occur between 380 and 400 K (Figure 5). In agreement with the absence of crystal water in **1**, a thermal event is observed by neither DSC nor X-ray diffraction in this temperature range. Whereas the thermal behaviors of **1** and **2** show obvious similarities in the temperature range above 420 K, the temperature response of **3** differs significantly. Between 440 and 460 K, an accurately defined exothermic decomposition reaction is observed for salts **1** and **2** that is associated with an amorphization of the samples. At temperatures above 580

**Scheme 2. Possible Reaction Pathway Drawn Exemplarily for the Thermal Decomposition of Ammonium Tricyanomelaminate 1**[a]

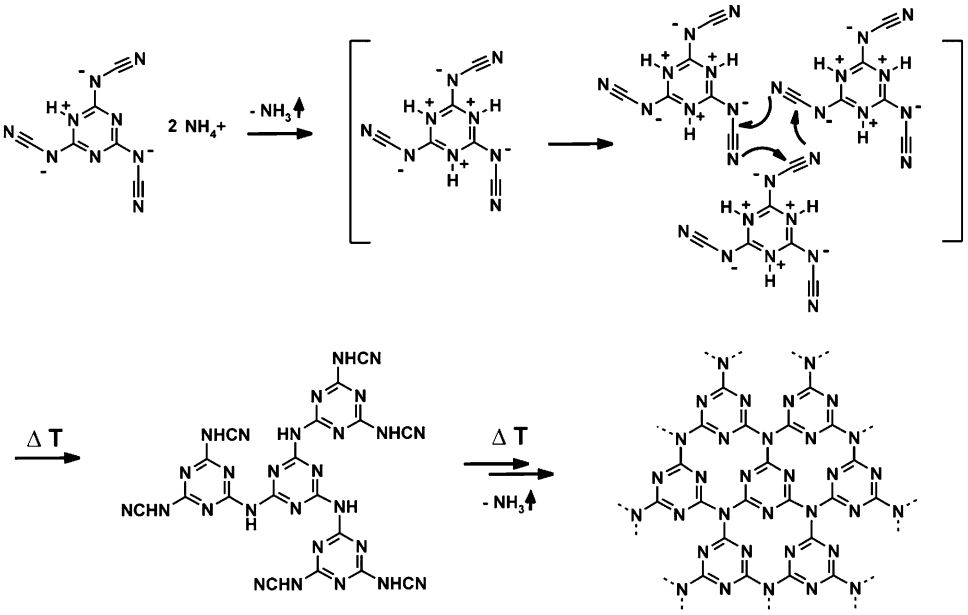


[a] According to this simplified scheme, the tricyanomelamine free acid undergoes polymerization, yielding an extended triazine-based network.

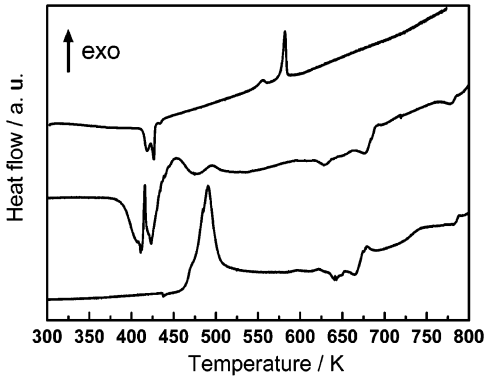


**Figure 4.** DSC curves recorded between room temperature and 800 K for **1** (bottom), **2** (middle), and **3** (top).

K, a succession of exothermic and endothermic signals is visible in the DSC curves, which, on the basis of the X-ray data, are likely to originate from the same underlying decomposition processes. Thus, at 620 K, a crystalline phase begins to form that is easily identified as melem, a prototypical heptazine-based $CN_x$ precursor.[39] Prior to the formation of melem, the reflections of another phase emerge around 550 K, with the latter being familiar from decomposition studies of melamine.[39,64] The identity of the latter phase, which is assumed to be composed of both melamine and melem,[64] will be the subject of a forthcoming paper. However, no evidence was found for the formation of single-phase melamine to a significant extent throughout the pyrolyses of both **1** and **2** by TPXRD. At 770 K, **1** and **2** transform into a semicrystalline phase with a relatively broad reflection at $2\theta \approx 12.1°$ ($\approx$ 336 pm, Mo K$\alpha$1 radiation), which is characteristic of graphitic carbon nitride materials.[35−37,64] Melaminium−TCM (**3**) exhibits a succession of solid−solid transitions between crystalline phases commencing at 380 K, whereas beyond 580 K, the sample becomes essentially X-ray amorphous. At temperatures around 700 K, a broad reflection at $2\theta \approx 12.1°$ indicates the formation of a disordered layered $CN_xH_y$ structure. As opposed to the thermolyses of **1** and **2**, neither melamine nor melem are observed as crystalline intermediates, which is supported by the lack of thermal events characteristic of melamine above 600 K in the DSC curve of **3**.

**IR Spectroscopy.** Vibrational spectroscopy was utilized as a probe for structural aspects of the quasi-amorphous intermediates of the thermal decomposition reactions. As evidenced by the pyrolysis behavior recorded by thermal analysis and TPXRD measurements (Figures 4 and 5), the crystalline transformation products passed through by **1** and **2** at temperatures $\geq$500 K, which are associated with a breakdown of the cyanamide moieties as well as a deprotonation of the triazine rings in **1**, are essentially identical. Because a marked difference in the high-temperature thermal behavior is only observed for **3** in the TPXRD measurements, the following discussion will be focused on the thermal decomposition of **2** and **3**. The measurements were performed on samples heated to the respective temperatures in sealed glass or quartz ampules. The composition of the resulting graphitic materials according to elemental analysis was as follows: C, 34.49; N, 61.38; H, 1.86 for **2**; and C, 35.45; N, 62.42; H, 1.72 for **3**, with the difference from a total of 100 wt % being presumably due to the presence of small amounts of oxygen. Contrasting the sequence of spectra obtained for **2** (Figure 6, left) and **3** (Figure 6, right), we may point out the following noticeable aspects:

As **2** is heated, the bands characteristic of both the tricyanomelaminate core and the cyanamide moiety decrease continuously. However, the sharp band around 800 $cm^{-1}$ featuring the ring breath vibration typical of both triazine and heptazine cores persists, though slightly broadened, throughout the decomposition process. Interestingly, the formation of melem is indicated already around 500 K by the appearance of a strong absorption around 1610 $cm^{-1}$, a

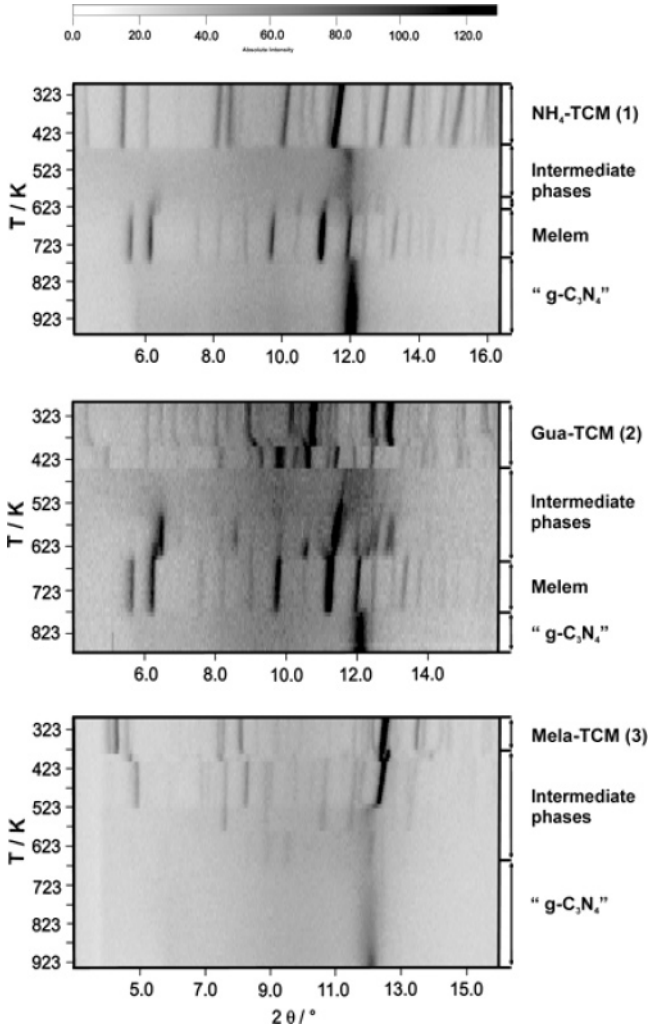


**Figure 5.** In situ temperature-dependent X-ray diffraction measurements (Mo $K_{\alpha 1}$ radiation) recorded between room temperature and $T > 850$ K. Whereas the decomposition pathways of **1** and **2** show evident similarities, that of **3** differs significantly in the medium-temperature regime. All patterns are dominated at high temperatures by a broad reflection at $2\theta \approx 12.1°$ (d $\approx$ 336 pm).

minor absorption at 1107 $cm^{-1}$, and the disappearance of the guanidinium and TCM bands at 1669 and 1390 $cm^{-1}$, respectively. The band at 1475 $cm^{-1}$ splits into a broad doublet originating from the triamino−heptazine (melem) vibrations. At 550 K, the spectrum is almost entirely dominated by the heptazine vibrations, with the low-energy flank being slightly broadened (1350−1200 $cm^{-1}$), thus mapping the envelope of the high-temperature absorption pattern. The well-resolved spectrum at 740 K shows strong absorption between 1636 and 1240 $cm^{-1}$ as well as the ring breath at 809 $cm^{-1}$, suggesting that the polymeric material is fairly well-ordered on a molecular level.

Although the thermal behavior of melaminium tricyanomelaminate (**3**) appears to be largely equivalent, amorphization commences earlier, leading to the rapid disappearance of the $\nu$(C≡N) vibrations and, notably, to a significant broadening in the $\nu$(C−N) region around 1320 $cm^{-1}$ at temperatures as low as 500 K. This feature is accompanied by pronounced absorption around 1620, 1550, and 1440 $cm^{-1}$, with the pattern reminiscent of the triazine absorption as found in melamine. Simultaneously, the characteristic ring breath that is located at 782 $cm^{-1}$ in the starting material is shifted to 807 $cm^{-1}$, thus substantiating the deprotonation of the initially monoprotonated triazine rings. The essence of the above observations may be interpreted in line with the formation of an intermediate low-temperature phase, exhibiting a significant degree of cross-linking between intact triazine cores, as indicated by the pronounced absorption below 1400 $cm^{-1}$. Low thermal stability of this intermediate phase is inferred by its facile conversion into melem above 580 K when the heat treatment in sealed glass ampules is extended to several hours. Thus, the thermal decomposition behavior of **3** may be rationalized by assuming significantly differing decomposition pathways under kinetic or thermodynamic control, the gradual shift between which leads to the superposition of features characteristic of both the assumed polymeric low-temperature phase and melem. Therefore, although neither melamine nor melem was detected by thermoanalytical and in situ X-ray investigations of **3**, the successive formation of both precursors could unambiguously be established when conducting the reaction in ampules under the pressure of ammonia. This is in accord with previous studies,[53] in which thermodynamically controlled reactions leading to the formation of melem are predominantly encountered when working in closed systems under $NH_3$ back pressure. Despite the different low-temperature decomposition behavior of **2** and **3**, the final decomposition products of **2** and **3** are essentially identical, as demonstrated by their IR spectra (Figure 6, top). As further evidenced by the respective XRD patterns (Figure 7), the high-temperature decomposition products exhibit a pronounced graphitic character, with the single reflection at $2\theta = 27.7-27.9°$ corresponding to an interlayer distance of ∼320 pm (the discrepancy with the d-value stated above (12.1° ≡ 336 pm) was not found to be an intrinsic effect but rather a result from a temperature shift of the lattice parameters).

**Solid-State NMR.** $^{15}N$ CP-MAS solid-state NMR experiments were carried out with the high-temperature decomposition products of **2** and **3**. The latter are shown in Figure 8 (**2**, bottom; **3**, middle), together with the decomposition product of $^{15}N$ melamine (top), all of which were obtained in sealed quartz ampules at 740 K (**2**) and 890 K (melamine and **3**). Despite the semi-amorphous character of all products, which are characterized by their X-ray powder patterns exhibiting only one single sharp reflection around 27.8° $2\theta$ (Figure 7), the appearance of their NMR spectra is strikingly well-resolved and, at the same time, largely identical. A similar reaction product of melamine and **2** may be ascribed to the favored formation of melem as a high-temperature crystalline intermediate observed during the pyrolyses of both melamine and **2** under various conditions (Figures 4 and 5). Thus, the spectral features in both cases simply represent the decomposition product of melem, though obtained at different temperatures. Notably, as indicated previously when discussing the vibrational spectra (Figure 6), comparison with the middle spectrum reveals that the decomposition of **3** yields the same product, which could not be anticipated solely on the basis of the DSC and TPXRD measurements. This adds to the interpretation of the thermal conversion of

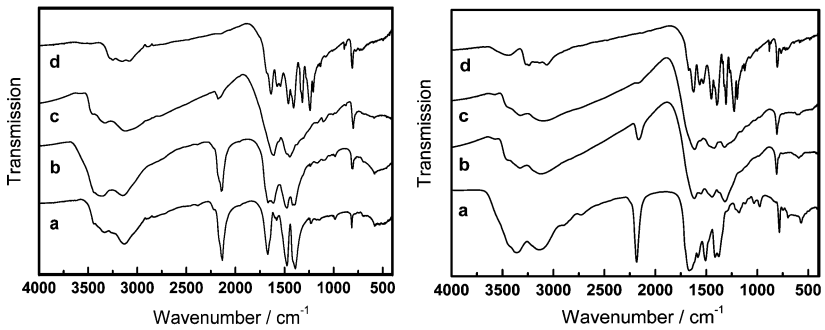


**Figure 6.** IR spectra of **2** (left) and **3** (right) before (a) and after thermal treatment in sealed glass ampules. Sample spectra are shown for the decomposition products at 470 (b), 550 (c), and 740 K (d) for **2** and at 500 (b), 570 (c), and 890 K (d) for **3**.

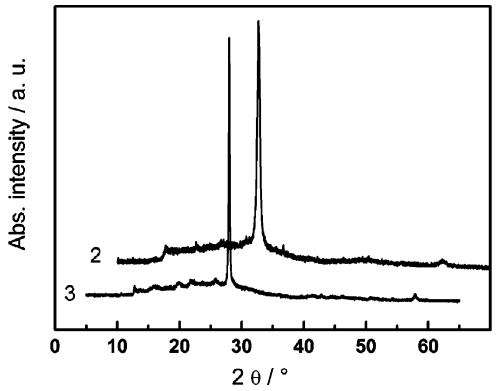


**Figure 7.** X-ray powder patterns (Cu $K_{\alpha 1}$ radiation) of the final decomposition products of **2** (top) and **3** (bottom). The top curve is drawn with an offset of 5° 2$\theta$ with respect to the bottom curve. Both materials exhibit a similar pattern of broad low-intensity peaks between 10 and 27° 2$\theta$ and a single sharp reflection at ~27.8° 2$\theta$, which corresponds to an average interlayer distance of approximately 320 pm.

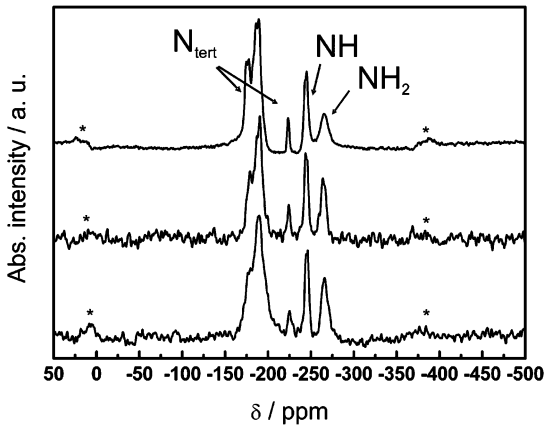


**Figure 8.** $^{15}N$ CP-MAS solid-state NMR spectra of the final decomposition products of **2** (740 K, bottom) and **3** (890 K, middle). In the top spectrum, the pyrolysis product of $^{15}N$-enriched melamine at 890 K is shown. Spinning sidebands are denoted with an asterisk; the rotation frequency was 10 kHz.

**3** proceeding via melem, if thermodynamic conditions ($NH_3$ back pressure, high temperature, long reaction time) can be premised. A qualitative interpretation of the isotropic chemical shifts observed can be put forward by analogy with the $^{15}N$ CP-MAS NMR spectra of the model systems melem and melamine, as discussed previously by Jürgens et al.[39] First, comparison of the basic signal patterns allows for the differentiation into tertiary (−195 and −225 ppm), secondary (NH, −246 ppm), and $NH_2$ (−266 ppm) nitrogen atoms, which is clearly supported by CPPI measurements using the decomposition product (Figure 8, top) of a $^{15}N$-enriched sample of melamine. Second, a noteworthy similarity between the chemical-shift spectrum of melem and that of the decomposition products of **1**−**3** is evident, on the basis of which the assignment of the signals in Figure 8 is feasible. In particular, the unique $N_{tert}$ resonance at −225 ppm, which is located at −234 ppm in melem but is absent in the spectrum of melamine, is likely to represent the central nitrogen atom of condensed heptazine cores.

According to these findings, the heptazine-based structure of melem is likely to be preserved in the final products, yet further evidence is necessary to unambiguously exclude the triazine-based model. A detailed solid-state NMR investigation of the graphitic decomposition products is currently underway in our group and will be published elsewhere.

## Discussion

The thermal decomposition of the tricyanomelaminate salts presented in this paper appears to be markedly different from that of metal-containing TCMs.[64] Whereas the latter have been found to become completely X-ray amorphous at elevated temperatures, leading to unidentified products,[58,60,64] a common well-defined reaction product was obtained for compounds **1**−**3**. Combined diffraction, thermoanalytical, and spectroscopic investigations indicate that layered $CN_xH_y$ materials can be formed as high-temperature decomposition products, corresponding to those commonly denoted as graphitic carbon nitride in the literature.

As for the correlation of the local structure of the pyrolysis products with that of the starting materials, evidence is put forward for the transformation of the triazine building blocks into heptazine rings as a result of thermal condensation processes. This fact can unambiguously be derived from the TPXRD patterns recorded for **1** and **2**, where melem is observed as a high-temperature crystalline phase between 650 and 770 K. For **3**, however, reflections pertaining to melem are absent in the TPXRD measurements, and the intermediate formation of a hypothetical metastable, triazine-based networked phase at low temperatures may tentatively be inferred on the basis of IR spectroscopic investigations.

Principally, though differing markedly in the low-temperature region, the decomposition pathway of **3** appears to gradually conform to that observed for **1** and **2** at elevated temperatures and $NH_3$ back pressure. Thus, decomposing **3** in closed systems clearly promotes the formation of melamine and melem, ultimately leading to a reaction product identical with those obtained from **1** and **2**. The conservation of the triazine units at temperatures beyond ~600 K can therefore be negated under the reaction conditions applied here, even if a preformed, purely triazine-based structure is used as molecular precursor. This is particularly noteworthy in the case of **3**, which is composed of potentially nucleophilic melamine units as well as tricyanomelaminate rings containing electrophilic cyanamide moieties, both of which may be capable of mutually interlinking upon heating. The thermodynamically favored formation of melem therefore seems to be the driving force dominating the thermal reactivity of $CN_x$-based precursors in the high-temperature regime, suggesting that purely triazine-based structures become unstable and essentially yield layered compounds made from heptazine building blocks. Preliminary solid-state NMR investigations are in line with this hypothesis, supporting a structure type of the graphitic $C_3N_4$ materials based on condensed heptazine rings, forming layers that are terminated by NH and $NH_2$ groups. However, whether the resulting polymer is identical with melon $[C_6N_7(NH_2)(NH)]_n$ ($\equiv [C_2N_3H]_n$), or whether the graphitic carbon nitride material is based on a larger 2D polymer of only partly condensed heptazine cores and frequent $NH/NH_2$ terminations within the layers, or whether extended sheets of fully condensed heptazines are formed that are terminated by NH and $NH_2$ groups at the layer-edges, can only be answered satisfactorily after further investigations.

## Conclusion

In this work, the crystal structures as well as characterization of the thermal reactivity of three novel tricyanomelaminates is reported. Ammonium, guanidinium, and melaminium tricyanomelaminate were discussed with respect to their suitability as potential $CN_x$ precursor materials, with the focus on the respective decomposition pathways. The pyrolyses were found to be uniform at high temperatures, all of which yielded melem as a common crystalline intermediate prior to the formation of a $CN_xH_y$ material that exhibited a layered, graphite-type structure. The obviously inevitable passage of the heptazine-based compound melem, though starting from purely triazine-based structures, strongly suggests that g-$C_3N_4$ materials composed of triazine motifs are kinetically labile with respect to the conversion into heptazine-based structures. Therefore, we believe the latter represents the thermodynamically stable modification of g-$C_3N_4$ at elevated temperatures.

**Acknowledgment.** We thank W. Wünschheim for conducting the DSC measurements, as well as Dr. P. Mayer, Dr. O. Oeckler, and T. Miller for collecting the single-crystal X-ray data. The authors gratefully acknowledge financial support that was granted from the Fonds der Chemischen Industrie, the BMBF, and the Studienstiftung des Deutschen Volkes (scholarships for B. V. Lotsch).

**Supporting Information Available:** X-ray crystallographic information files (CIF) and tables of atomic coordinates, anisotropic displacement parameters, and bond lengths and angles for ammonium tricyanomelaminate (**1**), guanidinium tricyanomelaminate hydrate (**2**), and melaminium tricyanomelaminate hydrate (**3**). This material is available free of charge via the Internet at http://pubs.acs.org.

CM052342F